 CMES, vol.20, no.2, pp.85-98, 2007

An Investigation of Wave Propagation with High Wave Numbers via the Regularized LBIEM

H.B. Chen[1], D.J. Fu[1] and P.Q. Zhang[1]

Abstract: Researches today show that, both approximation and dispersion errors are encountered by classical Galerkin FEM solutions for Helmholtz equation governing the harmonic wave propagation, which leads to numerical inaccuracies especially for high wave number cases. In this paper, Local Boundary Integral Equation Method (LBIEM) is firstly implemented to solve the boundary value problem of Helmholtz equation. Then the regularized LBIE is proposed to overcome the singularities of the boundary integrals in the LBIEM. Owing to the advantages of the Moving Least Square Approximation (MLSA), the frequency-dependent basis functions modified by the harmonic wave propagation solutions are easily adopted instead of the normal monomial basis functions. A plane harmonic wave propagating case is examined in the numerical tests. Computational results show that excellent numerical accuracies can be obtained when the regularized formulation and the modified basis functions are adopted, even though the wave numbers of Helmholtz equation are high.

Keyword: Helmholtz equation; Local boundary integral equation method; Moving least square approximation; Regularization; Modified basis function

1 Introduction

It is well known that acoustic wave harmonically propagating problem is governed by Helmholtz equation, $\Delta u+\kappa^2 u=0$, where κ is the wave number. As the dominant numerical method, FEM solutions for boundary value problem of Helmholtz equation are widely investigated, for either interior or exterior problems. References [Ihlenburg, F. et al (1995a), Ihlenburg, F. et al (1995b), Deraemaeker, A. et al (1999)] show that numerical errors consist of approximation and dispersion errors, in particular, it can be shown here that relative error of the FE-solution defined by H^1-seminorm generally can be written as

$$e_1 \leq C_1 \kappa h + C_2 \kappa^3 h^2 \tag{1}$$

Here C_1 and C_2 are constants that are independent of the wave number κ and the mesh size h. The first term on the right of the inequation (1) represents the approximation error and the second one reflects the dispersion error. Obviously, with increasing wave number, dispersion error accordingly increases even if κh is kept constant and thus pollutes numerical accuracies.

For higher wave number cases, finer meshes and higher orders of FEs are necessarily adopted to reduce the approximation error and dispersion error, however, enormous computation scale usually makes the numerical solutions unreliable. Several methods are proposed to improve the classical FEM, such as Galerkin Least-square, Quasi-stabilized finite element method and Residual-free finite element method, etc. Nevertheless, these methods eliminate or minimize the dispersion error only in one dimensional problem but have not given desired numerical accuracies in higher dimensional cases, see references [Ihlenburg, F. et al (1995a), Suleau, S. et al (2000a)].

Developing meshless methods present us a new consideration. Melenk and Babuska (1997) firstly suggested the partition of unity, a vital meshless method, to solve the Helmholtz equation with high wave number. They suggested that 'generalized harmonic functions' share the optimality properties for the approximation of harmonic

[1] CAS Key Laboratory of Mechanical Behavior and Design of Materials, Department of Modern Mechanics, University of Science and Technology of China, Hefei, Anhui 230026, P.R. China. Email: hbchen@ustc.edu.cn

functions which are oscillatory. Similar treatments can be found in reference [Uras, R. et al (1997)], in which Uras et al. applied the reproducing kernel particle method to acoustics. Chen, W. et al. (2002, 2003) also introduced the meshfree boundary particle method and boundary knot method into Helmholtz problems, excellent results have been obtained even if wave numbers are very high. Bouillard and Suleau (1998) applied element free Galerkin method to the harmonic wave propagation problem of two dimensions for the first time, and numerical experiments showed that, for identical distribution of nodes, better accuracies were obtained with the optimal choice of parameters in the MLSA. Furthermore, they modified normal basis functions with plane harmonic wave propagation solutions and presented the primary proof and numerical assessment on minimizing the dispersion error in one and two dimensional problems [Suleau, S. et al (2000b), Suleau, S. et al (2000a)]. High accuracies were obtained in numerical tests especially for high wave number cases.

In this paper, LBIEM [Zhu, T. L. et al (1998), Zhu, T. L. et al (1999)] is addressed to solve the Helmholtz equation of two dimensional problems. LBIEM is a significant and adoptable meshless method, which can be regarded as a special Meshless Local Petrov-Galerkin (MLPG) approach where its test functions are derived from fundamental solutions in BEM [Atluri, S. N. et al (1998), Han, Z. D. et al (2003), Han, Z. D. et al (2005)]. Compared with EFGM, it needs no background meshes for the integration, thus is a so-called truly meshless method, and it has been widely applied to potential problems, elastostatics, elastodynamics, thermoelasticity, plate bending problems, and so on [Sladek, J. et al (2002a), Sladek, J. et al (2005)]. LBIEM adopts Moving Least Square Approximation (MLSA) in which some characteristic functions related to the physical problems can be readily furnished in the basis function series. For instance, such idea can be found in reference [Sladek, V. et al (2005)] with solutions for non-homogeneous problems. LBIEM solutions for the equation of Helmholtz type are firstly introduced by Zhu et al (1999) to show convenience for volume integration, which is normally troublesome because of the non-linear term. For the boundary value problem of Helmholtz equation, Sladek et al (2002b) investigated the sound vibration problems based on non-singular global and local Trefftz boundary integral formulations. In the present paper, some basic parameters, for example, the choices of the size of the influence domain, are considered firstly, and normal linear basis functions are then modified by the wave propagation solutions in the MLSA process, which can locally approximate the acoustic field potential accurately. The regularized LBIEs are introduced to eliminate the singularity when the sourse node locates on the global boundary. Finally, numerical experiments reveal that excellent numerical accuracies and convergences can be obtained even for high wave number problems.

The following discussion begins with the description of LBIE and its regularization in section 2. Section 3 focuses on MLSA with normal and modified basis functions. The discretization and numerical implementation scheme are presented in section 4. A two-dimensional plane harmonic wave propagation problem, as the numerical test, is given in section 5. The article ends with some conclusions in section 6.

2 Local boundary integral equation and regularization

The acoustic wave harmonically propagating problem can be addressed by the potential boundary value problem of Helmholtz equation as follows:

$$\begin{cases} \nabla^2 u(\mathbf{x}) + \kappa^2 u(\mathbf{x}) = 0 & \mathbf{x} \in \Omega \\ u = \overline{u} & \text{on } \Gamma_u \\ q = \frac{\partial u}{\partial n} = \overline{q} & \text{on } \Gamma_q \end{cases} \tag{2}$$

where u is the potential function according to the acoustic pressure of sound field Ω that is enclosed by $\Gamma = \Gamma_u \cup \Gamma_q$, as shown in Fig. 1. $\kappa = \omega/c$ is the wave number with ω and c the frequency and velocity of wave propagation, respectively. Here $\overline{u}$ is prescribed potential on Dirichlet boundary Γ_u and $\overline{q}$ is prescribed normal flux on Neumann

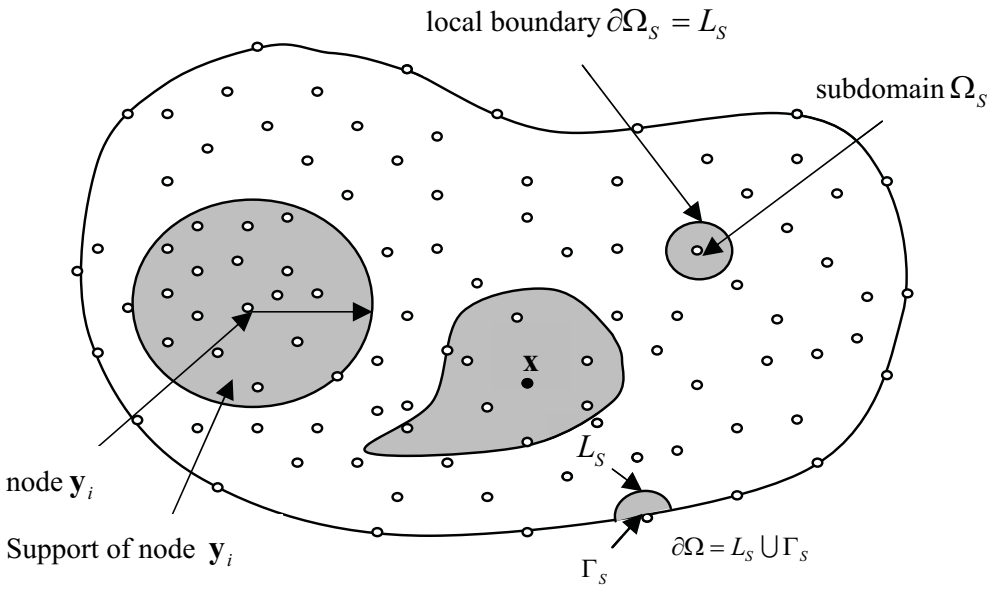

Figure 1: Local boundary, support of nodes, domain of influence of a source point, and so on, see reference [Zhu T. L. et al (1998)]

boundary Γ_q, n is the outward normal direction to the boundary Γ. Note that complex expressions are more general in the sound field formulae and boundary conditions, and combined boundary condition, i.e., robin boundary conditions, are more common especially for exterior problems.

A weak formulation of Helmholtz equation can be written as,

$$\int_\Omega u^* \left(\nabla^2 u(\mathbf{x}) + \kappa^2 u(\mathbf{x})\right) = 0 \tag{3}$$

where u^* is the test function and u is the trail function. Two choices of test function can be introduced in the LBIEM, either

$$\nabla^2 u^*(\mathbf{x},\mathbf{y}) + \delta(\mathbf{x},\mathbf{y}) = 0 \tag{4}$$

or

$$\nabla^2 u^*(\mathbf{x},\mathbf{y}) + \kappa^2 u(\mathbf{x},\mathbf{y}) + \delta(\mathbf{x},\mathbf{y}) = 0 \tag{5}$$

with $\delta(\mathbf{x},\mathbf{y})$ being the Dirac delta function. Considering volume integral is so convenient in the LBIEM that Eq. (4) can be employed here to avoid the complex Hankel function in the integral kernel functions.

After integration by parts and application of Eq. (4), the following integral equation can be obtained,

$$u(\mathbf{y}) = \int_\Gamma u^*(\mathbf{x},\mathbf{y}) \frac{\partial u(\mathbf{x})}{\partial n} d\Gamma - \int_\Gamma \frac{\partial u^*(\mathbf{x},\mathbf{y})}{\partial n} u(\mathbf{x}) d\Gamma + \int_\Omega u^*(\mathbf{x},\mathbf{y}) \kappa^2 u(\mathbf{x}) d\Omega \tag{6}$$

where n is outward normal direction to the boundary, $\mathbf{x}$ is a field point and $\mathbf{y}$ the source point. Instead of global domain Ω of the given problem, Eq. (6) should hold over the sub-domain Ω_S which is entirely located inside Ω and contain the source point $\mathbf{y}$,

$$u(\mathbf{y}) = \int_{\partial\Omega_S} u^*(\mathbf{x},\mathbf{y}) \frac{\partial u(\mathbf{x})}{\partial n} d\Gamma - \int_{\partial\Omega_S} \frac{\partial u^*(\mathbf{x},\mathbf{y})}{\partial n} u(\mathbf{x}) d\Gamma + \int_{\Omega_S} u^*(\mathbf{x},\mathbf{y}) \kappa^2 u(\mathbf{x}) d\Omega \tag{7}$$

where $\partial\Omega_s$ is the boundary of the sub-domain Ω_s. If source point $\mathbf{y}$ locates on the global boundary, LBIE can be obtained similar to global BIE of the classic BEM, as follows,

$$\alpha(\mathbf{y}) u(\mathbf{y}) = \int_{L_S+\Gamma_S} u^*(\mathbf{x},\mathbf{y}) \frac{\partial u(\mathbf{x})}{\partial n} d\Gamma - \int_{L_S+\Gamma_S} \frac{\partial u^*(\mathbf{x},\mathbf{y})}{\partial n} u(\mathbf{x}) d\Gamma + \int_{\Omega_S} u^*(\mathbf{x},\mathbf{y}) \kappa^2 u(\mathbf{x}) d\Omega \tag{8}$$

where Γ_S is the part of local boundary $\partial\Omega_S$, which coincides with the global boundary Γ, i.e., $\Gamma_S = \partial\Omega_S \cap \Gamma$. L_S is the part of local boundary $\partial\Omega_S$ inside Ω, and

$$\alpha(\mathbf{y}) = \begin{cases} 1/2 & \text{for } \mathbf{y} \text{ located on the smooth boundary} \\ \theta/(2\pi) & \text{for } \mathbf{y} \text{ located on the boundary corner} \end{cases} \tag{9}$$

with θ being the internal angle of boundary corner.

Over the sub-domains, the modified test function with the companion solution given by [Zhu, T. L. et al (1998)] can be utilized here, i.e.,

$$u^{**} = u^* - u' = \frac{1}{2\pi}\ln\frac{1}{r} - \frac{1}{2\pi}\ln\frac{1}{r_0} = \frac{1}{2\pi}\ln\frac{r_0}{r} \tag{10}$$

where $r = |\mathbf{x}-\mathbf{y}|$ denotes the distance from the source point to the field point, and r_0 is the radius of local sub-domain. Replace u^* with u^{**} in Eqs. (7) and (8), or use u^{**} as a new test function in Eq. (3) and integrate by parts twice, then note that $-\nabla^2 u^{**} = -\nabla^2 u^* + \nabla^2 u' = \delta(\mathbf{x},\mathbf{y})$ in Ω_S and $u^{**} = 0$ along $\partial\Omega_S$, we can obtain the LBIEs of LBIEM, as

$$u(\mathbf{y}) = -\int_{\partial\Omega_S} \frac{\partial u^{**}(\mathbf{x},\mathbf{y})}{\partial n} u(\mathbf{x}) d\Gamma + \int_{\Omega_S} u^{**}(\mathbf{x},\mathbf{y})\kappa^2 u(\mathbf{x}) d\Omega \tag{11}$$

for source point inside Ω, and

$$\alpha(\mathbf{y})u(\mathbf{y}) = \int_{\Gamma_s} u^{**}(\mathbf{x},\mathbf{y})\frac{\partial u(\mathbf{x})}{\partial n} d\Gamma - \int_{L_S+\Gamma_s} \frac{\partial u^{**}(\mathbf{x},\mathbf{y})}{\partial n} u(\mathbf{x}) d\Gamma + \int_{\Omega_S} u^{**}(\mathbf{x},\mathbf{y})\kappa^2 u(\mathbf{x}) d\Omega \tag{12}$$

for source point on the global boundary Γ.

It should be noted that the first term on the right of Eq. (12) is weakly singular and the second one is strongly singular [Sellountos, E. J. et al (2005), Sladek, V. et al (2000)]. For integration with weak singularity, one can adopt the logarithmic quadrature to achieve high accuracies, but strongly singular term should be specially treated with, for example, using the regularization technique which is simple and efficient [Chen, H. B. et al (1998), Chen, H. B. et al (2001), Chen, H. B. et al (2003), Guo, X. F. et al (2006a), Guo, X. F. et al (2006b)].

Based on the knowledge of classic BEM, the following expression holds,

$$\alpha(\mathbf{y}) = -\int_{L_S+\Gamma_S} \frac{\partial u^{**}(\mathbf{x},\mathbf{y})}{\partial n} d\Gamma \tag{13}$$

Furthermore,

$$\alpha(\mathbf{y})u(\mathbf{y}) = -\int_{L_S+\Gamma_S} \frac{\partial u^{**}(\mathbf{x},\mathbf{y})}{\partial n} u(\mathbf{y}) d\Gamma \tag{14}$$

Subtracting Eq. (14) from Eq. (12), we have

$$0 = \int_{\Gamma_s} u^{**}(\mathbf{x},\mathbf{y})\frac{\partial u(\mathbf{x})}{\partial n} d\Gamma - \int_{L_S+\Gamma_s} \frac{\partial u^{**}(\mathbf{x},\mathbf{y})}{\partial n}(u(\mathbf{x}) - u(\mathbf{y})) d\Gamma + \int_{\Omega_S} u^{**}(\mathbf{x},\mathbf{y})\kappa^2 u(\mathbf{x}) d\Omega \tag{15}$$

Eq. (15) is called the regularized LBIE. Here $\frac{\partial u^{**}(\mathbf{x},\mathbf{y})}{\partial n} = O(r^{-1})$ and $u(\mathbf{x}) - u(y) = O(r)$ as $\mathbf{x} \to \mathbf{y}$, thus, the strong singularity in Eq. (15) can be eliminated.

Eqs. (11) and (12) are the LBIEs in the implementation of original LBIEM while Eqs. (11) and (15) are those of regularized LBIM.

3 Normal and modified basis functions in the MLSA

Moving least square approximation (MLSA) is the pioneer and significant approximation method in the evolution of meshless methods, which is based on the values (the fictitious values, further) of the discrete nodes that are regularly or randomly distributed. For node $\mathbf{x}$, the trial function, in other word, locally approximate function $u^h(\mathbf{x})$ of $u(\mathbf{x})$, can be defined by

$$u^h(\mathbf{x}) = \sum_{i=1}^{m} p_i(\mathbf{x}) \cdot a_i(\mathbf{x}) = \mathbf{p}^T(\mathbf{x}) \cdot \mathbf{a}(\mathbf{x}) \quad (\mathbf{x} \in \Omega_x) \tag{16}$$

where $\mathbf{p}^T(\mathbf{x}) = [p_1(\mathbf{x}), p_2(\mathbf{x}), \cdots, p_m(\mathbf{x})]$ is a complete monomial basis of order m, and $\mathbf{a}(\mathbf{x})$ is the vector containing coefficients $a_i(\mathbf{x})$, $i = 1, 2, \cdots, m$. For two dimensional problems, normal linear basis is $\mathbf{p}^T(\mathbf{x}) = (1, x_1, x_2)$, $m = 3$, and normal quadratic basis is $\mathbf{p}^T(\mathbf{x}) = (1, x_1, x_2, (x_1)^2, x_1x_2, (x_2)^2)$, $m = 6$.

For the harmonic wave propagation problem, other basis functions seem to be more suitable than the normal monomial basis functions [Suleau, S. et al (2000a), Babuska, I. et al (1997)]. For two dimensional case of plane wave, we can use modified normal basis functions, $\mathbf{p}^T(\mathbf{x}) = \{1, \cos(\kappa x_1 \cos\beta + \kappa x_2 \sin\beta), \quad \sin(\kappa x_1 \cos\beta + \kappa x_2 \sin\beta), \quad \cos(-\kappa x_1 \sin\beta + \kappa x_2 \cos\beta), \sin(-\kappa x_1 \sin\beta + \kappa x_2 \cos\beta)\}$. The modified basis functions are also called the frequency-dependent ones in reference [Suleau, S. et al (2000a)]. Obviously, to adopt modified basis functions, there exist more locally approximate advantages than the normal basis ones, which is especially important for the high wave number cases. When being used to numerically solve the Helmholtz equation, classical FEM requires special element dense per wavelength to control the approximation error, which usually leads to large numbers of elements and nodes to be imposed for high wave number cases. MLSA with modified basis functions possesses high approximation accuracies in spite of high wave number cases within special limits, for instance, nodes in the support or special frequency range [Ihlenburg, F. et al (1995b)]. To our joy, the dispersion error is also remarkably eliminated with adoption of the modified basis functions [Suleau, S. et al (2000b), Suleau, S. et al (2000a)], however, theoretical research needs more.

The coefficient vector $\mathbf{a}(\mathbf{x})$ is determined by minimizing a weighted discrete L_2 norm, defined as

$$J(\mathbf{x}) = \sum_{i=1}^{n} w_i(\mathbf{x})[\mathbf{p}^T(\mathbf{x}_i)\mathbf{a}(\mathbf{x}) - \hat{u}_i]^2 = (\mathbf{Pa} - \hat{\mathbf{u}})^{\mathbf{T}}\mathbf{W}(\mathbf{x})(\mathbf{Pa} - \hat{\mathbf{u}}) \quad (17)$$

where $w_i(\mathbf{x})$ is the weight function associated with node i, and $\hat{u}_i$ are the fictitious node values different from the node values of the unknown trial function $u^h(\mathbf{x})$ in general.

The stationarity of $J(\mathbf{x})$ in Eq. (17) with respect to $\mathbf{a}(\mathbf{x})$ leads to the following linear relationship between $\mathbf{a}(\mathbf{x})$ and $\hat{\mathbf{u}}$,

$$\mathbf{A}(\mathbf{x})\mathbf{a}(\mathbf{x}) = \mathbf{B}(\mathbf{x})\hat{\mathbf{u}} \quad (18)$$

where matrices $\mathbf{A}(\mathbf{x})$ and $\mathbf{B}(\mathbf{x})$ are defined by

$$\mathbf{A}(\mathbf{x}) = \mathbf{P}^{\mathbf{T}}\mathbf{W}(\mathbf{x})\mathbf{P} = \sum_{i=1}^{n} w_i(\mathbf{x})\mathbf{p}(\mathbf{x}_i)\mathbf{p}^T(\mathbf{x}_i) \quad (19)$$

$$\mathbf{B}(\mathbf{x}) = \mathbf{P}^{\mathbf{T}}\mathbf{W}(\mathbf{x}) = [w_1(\mathbf{x})\mathbf{p}(\mathbf{x}_1), w_2(\mathbf{x})\mathbf{p}(\mathbf{x}_2), \ldots, w_n(\mathbf{x})\mathbf{p}(\mathbf{x}_n)] \quad (20)$$

A necessary condition for a well-defined MLSA is that at least m weight functions are non-zero (i.e. $n \geq m$) for each sample point.

Solving for $\mathbf{a}(\mathbf{x})$ from Eq. (18) and substituting it into Eq. (16), then the final approximation formula can be obtained as

$$u^h(\mathbf{x}) = \mathbf{\Phi}^T(\mathbf{x})\hat{\mathbf{u}} = \sum_{i=1}^{n} \Phi_i(\mathbf{x})\hat{u}_i \quad u^h(\mathbf{x}_i) = u_i \neq \hat{u}_i \quad (21)$$

where

$$\mathbf{\Phi}^T(\mathbf{x}) = [\Phi_1(\mathbf{x}), \Phi_2(\mathbf{x}), \ldots, \Phi_n(\mathbf{x})] = \mathbf{p}^{\mathbf{T}}(\mathbf{x})\mathbf{A}^{-\mathbf{1}}(\mathbf{x})\mathbf{B}(\mathbf{x}) \quad (22)$$

$\Phi_i(\mathbf{x})$ is called shape functions of the MLSA, the smoothness of which is determined by that of the basis functions and of the weight functions.

The partial derivatives of $\Phi_i(\mathbf{x})$,

$$\Phi_{i,k}(\mathbf{x}) = \sum_{j=1}^{m} p_{j,k}(A^{-1}B)_{ji} + p_j(A^{-1}B_{,k} + A^{-1}_{,k}B)_{ji} \quad (23)$$

In which $A^{-1}_{,k} = (A^{-1})_{,k}$ represents the derivative of the inverse of $\mathbf{A}$ with respect to x_k, which is given by

$$A^{-1}_{,k} = -A^{-1}A_{,k}A^{-1} \quad (24)$$

In our implementing the MLSA, the chosen Gaussian weight function corresponding to node i may be written as

$$\omega_i(\mathbf{x}, r_i) = \begin{cases} \frac{\exp[-(d/c_i)^{2k}] - \exp[-(r_i/c_i)^{2k}]}{1 - \exp[-(r_i/c_i)^{2k}]} & 0 \leq d \leq r_i \\ 0 & d \geq r_i \end{cases},$$

(25)

where $d = \|\mathbf{x} - \mathbf{x}_i\|$; c_i is a constant controlling the shape of the weight function w_i and therefore the relative weights; and r_i is the size of the support for the weight function w_i and determines the support of node $\mathbf{x}_i$. In present computation, $k = 1$ is chosen.

4 Discretization scheme

Substituting Eq. (21) into Eqs. (11) and (12), after imposing boundary condition on the right hand side for node i and carrying out numerical integration, the following equations may be obtained

$$\alpha_i u_i = f_i' + \sum_{j=1}^{n} K_{ij}' \hat{u}_j, i = 1, 2, \ldots, N \tag{26}$$

where N is the total number of nodes in the entire domain Ω; coefficientsα_i, $i = 1, 2, \ldots, N$, are

$$\alpha_i = \begin{cases} 1 & \text{for internal nodes} \\ 1/2 & \text{for } \mathbf{y} \text{ located on a smooth boundary} \\ \theta/(2\pi) & \text{for } \mathbf{y} \text{ located on a boundary corner} \end{cases} \tag{27}$$

with θ being the internal angle of the boundary corner. Then

$$\begin{cases} f_i' = 0 \\ K_{ij}' = -\int_{L_s} \Phi_j(\mathbf{x}) \frac{\partial u^{**}}{\partial n} d\Gamma + \int_{\Omega_S} u^{**} \kappa^2 \Phi_j(\mathbf{x}) d\Omega \end{cases} \tag{28}$$

for internal nodes, and

$$\begin{cases} f_i' = \int_{\Gamma_{sq}} u^{**} \overline{q} d\Gamma - \int_{\Gamma_{su}} \overline{u} \frac{\partial u^{**}}{\partial n} d\Gamma \\ K_{ij}' = \int_{\Gamma_{su}} u^{**} \frac{\partial \Phi_j(\mathbf{x})}{\partial n} d\Gamma - \int_{\Gamma_{sq}} \Phi_j(\mathbf{x}) \frac{\partial u^{**}}{\partial n} d\Gamma \\ \quad - \int_{L_s} \Phi_j(\mathbf{x}) \frac{\partial u^{**}}{\partial n} d\Gamma + \int_{\Omega_S} u^{**} \kappa^2 \Phi_j(\mathbf{x}) d\Omega \end{cases} \tag{29}$$

for boundary nodes, where Γ_{sq} and Γ_{su} are the flux and essential boundary sections of Γ_s with $\Gamma_s = \Gamma_{su} \cup \Gamma_{sq}$, and $\overline{u}$ is the prescribed potential at Γ_{su}, $\overline{q}$ is the prescribed flux at Γ_{sq}. L_s is a part of the local boundary $\partial\Omega$ which is not located on the global boundary Γ. For those interior nodes located inside the domainΩ, $L_s = \partial\Omega$, see Fig. 1.

It is very convenient to impose the essential boundary conditions on the left hand side of Eq. (26), and then we have the following linear system

$$\mathbf{K}\hat{\mathbf{u}} = \mathbf{f} \tag{30}$$

with the fictitious nodal values $\hat{\mathbf{u}}$ as unknowns, where the entries of $\mathbf{K}$ and $\mathbf{f}$ are given by

$$K_{ij} = \begin{cases} -K_{ij}' & \text{for nodes with } u_i \text{ prescribed} \\ -K_{ij}' + \alpha_i \phi_j(x_i) & \text{for nodes with } u_i \text{ unknown} \end{cases} \tag{31}$$

and

$$f_i = \begin{cases} f_i' - \alpha_i \overline{u}_i & \text{for nodes with } u_i \text{ prescribed} \\ f_i' & \text{for nodes with } u_i \text{ unknown} \end{cases} \tag{32}$$

For regularized LBIE, the discrete expressions are

$$\begin{cases} K_{ij}' = -\int_{\partial\Omega_s} \frac{u^{**}(\mathbf{x},\mathbf{y})}{\partial n} \phi_j(\mathbf{x}) d\Gamma \\ \qquad + \int_{\Omega_s} u^{**}(\mathbf{x},\mathbf{y}) \kappa^2 \phi_j(\mathbf{x}) d\Gamma \\ f_i' = 0 \end{cases} \tag{33}$$

for internal nodes, and for the nodes on the boundary,

$$\begin{cases} K_{ij}' = -\int_{L_S} \frac{\partial u^{**}(\mathbf{x},\mathbf{y})}{\partial n} \phi_j(\mathbf{x}) d\Gamma \\ + \int_{\Gamma_{su}} u^{**}(\mathbf{x},\mathbf{y}) \frac{\partial \phi_j(\mathbf{x})}{\partial n} d\Gamma - \int_{\mathrm{T}_{sq}} \frac{\partial u^{**}(\mathbf{x},\mathbf{y})}{\partial n} \phi_j(\mathbf{x}) d\Gamma \\ + \int_{\Omega_s} u^{**}(\mathbf{x},\mathbf{y}) \kappa^2 \phi_j(\mathbf{x}) d\Gamma \\ f_i' = -\int_{L_S} \frac{\partial u^{**}(\mathbf{x},\mathbf{y})}{\partial n} (-\overline{u}(\mathbf{y})) d\Gamma \\ - \int_{\Gamma_{su}} \frac{\partial u^{**}(\mathbf{x},\mathbf{y})}{\partial n} (\overline{u} - \overline{u}(\mathbf{y})) d\Gamma + \int_{\Gamma_{sq}} u^{**}(\mathbf{x},\mathbf{y}) \overline{q} d\Gamma \\ - \int_{\mathrm{T}_{sq}} \frac{\partial u^{**}(\mathbf{x},\mathbf{y})}{\partial n} (-\overline{u}(\mathbf{y})) d\Gamma \end{cases} \tag{34}$$

when the potential is known, and

$$\begin{cases} K_{ij}' = -\int_{L_S} \frac{\partial u^{**}(\mathbf{x},\mathbf{y})}{\partial n} (\phi_j(\mathbf{x}) - \phi_j(\mathbf{y})) d\Gamma \\ \qquad + \int_{\Gamma_{su}} u^{**}(\mathbf{x},\mathbf{y}) \frac{\partial \phi_j(\mathbf{x})}{\partial n} d\Gamma \\ \qquad - \int_{\Gamma_{su}} \frac{\partial u^{**}(\mathbf{x},\mathbf{y})}{\partial n} (-\phi_j(\mathbf{y})) d\Gamma \\ \qquad - \int_{\mathrm{T}_{sq}} \frac{\partial u^{**}(\mathbf{x},\mathbf{y})}{\partial n} (\phi_j(\mathbf{x}) - \phi_j(\mathbf{y})) d\Gamma \\ \qquad + \int_{\Omega_s} u^{**}(\mathbf{x},\mathbf{y}) \kappa^2 \phi_j(\mathbf{x}) d\Gamma \\ f_i' = -\int_{\Gamma_{su}} \frac{\partial u^{**}(\mathbf{x},\mathbf{y})}{\partial n} \overline{u} d\Gamma + \int_{\Gamma_{sq}} u^{**}(\mathbf{x},\mathbf{y}) \overline{q} d\Gamma \end{cases}$$

(35)

when the potential is unknown. Obviously, for the formulation of regularized LBIE, $\alpha_i \equiv 0$.

5 Numerical tests

In this chapter, numerical examples are firstly performed to show the original implementation of LBIEM for Helmholtz equation, and some fundamental parameters, e.g., sizes of the domain of influence, basis functions, are discussed. Comparisons among the linear basis functions, the quadratic basis functions and the modified basis functions are also implemented. Then an example with elliptical boundary is used to show the improvement in numerical accuracies after the LBIE is regularized. In the end, plane wave propagating through a two dimensional domain of car section with complex geometry boundary is adopted to test the computer codes of the regularized LBIEM with modified basis functions. For the purpose of error estimation and convergence studies, the semi-norm of Sobolev space,

$$|u|_1 = (\int_\Omega ((\frac{\partial u}{\partial x_1})^2 + (\frac{\partial u}{\partial x_2})^2) d\Omega)^{\frac{1}{2}} \tag{36}$$

is used to define the relative error,

$$e_r = \frac{|u^{num} - u^{exact}|_1}{|u^{exact}|_1} \times 100\% \tag{37}$$

where superscript *exact* and *num* denote exact and numerical solutions, respectively. To show the improving numerical accuracies of regularized LBIEM, the node relative error over node i is defined as

$$e_i = \frac{|u_i^{num} - u_i^{exact}|}{(\sum_i^n |u_i^{exact}|)/n} \times 100\% \tag{38}$$

The boundary values of all the numerical tests are described by exact solution,

$$u = \cos(\kappa x_1 \cos\beta + \kappa x_2 \sin\beta) \tag{39}$$

for the plane harmonic wave propagation problem.

5.1 Original LBIEM solutions for Helmholtz equation

In this section, a square domain with corresponding boundary conditions that potentials are known on the horizontal sides ($x_2 = \pm 1$) and flows are known on the vertical sides ($x_1 = \pm 1$), see Fig. 2. In the numerical implementation of LBIEM, the choices of parameters such as the size of the influence domain, radii of local sub-domain, or controlling constants of relative weights, etc., have special effect on the numerical accuracies. Therefore, the size of the influence domain, the plane wave propagating angle and the wave number are discussed here.

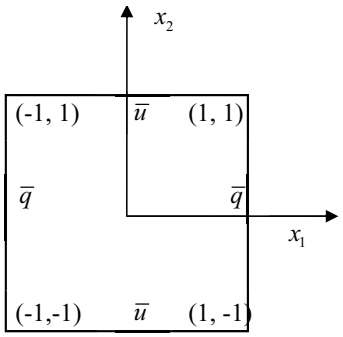

Figure 2: Test example of a square domain

5.1.1 Study on the size of the influence domain

Based on the present literatures of meshless methods, the radius of sub-domain $r_0 = 0.005$, and the ratio between the size of the influence domain and the controlling constant of the relative weight, i.e. $dinf/c \approx 4$, are used in the computation of all cases. Regularly distributed nodes of $36(6\times 6)$, $49(7\times 7)$, $64(8\times 8)$ and $81(9\times 9)$ are used to study numerical accuracies with respect to the size of the influence domain. Linear and modified basis functions are considered here. The plane wave propagating angle is set $\beta = 45^o$ and the wave number is set$\kappa = 1.0$. The ratio between the size of the influence domain and the distance of the two closest nodes is defined as $\alpha = dinf/h$. After keeping the coefficient matrix non-singular and the wave number under the cut-off value (see reference [Ihlenburg, F. et al (1995b)]), we can choose increasing ratios with

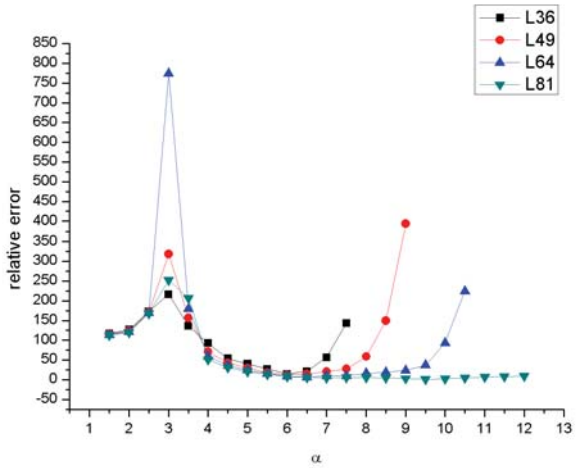

Figure 3: Relative error with respect to the size of influence domain, linear basis case

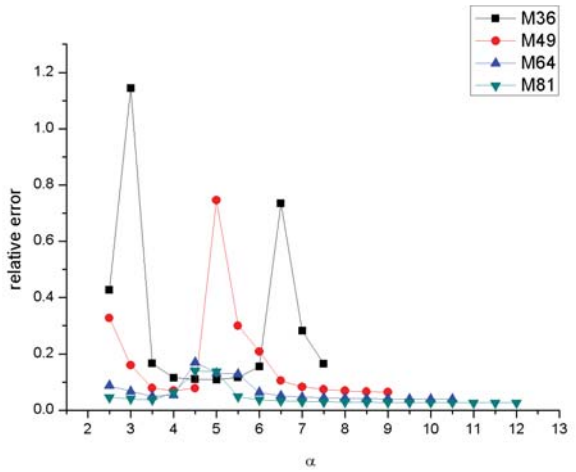

Figure 4: Relative error with respect to the size of influence domain, modified basis case

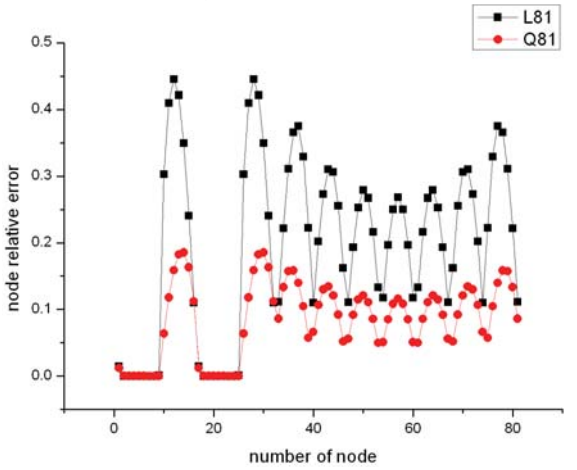

Figure 5: Comparison of the nodal errors between linear and quadric basis functions, $\kappa = 1$

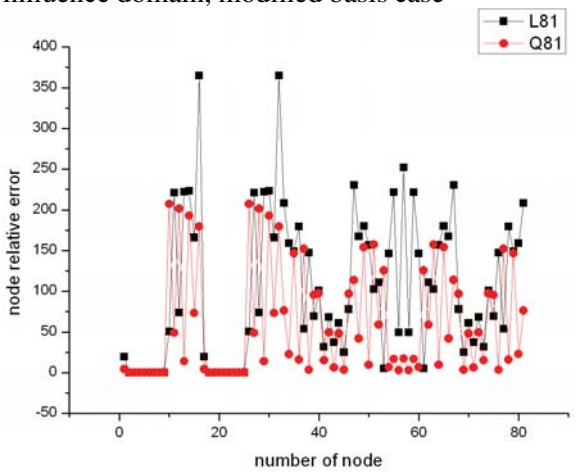

Figure 6: Comparison of the nodal errors between linear and quadric basis functions, $\kappa = 8$

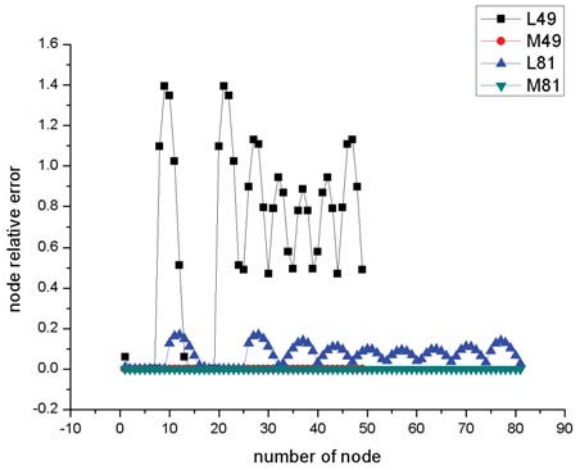

Figure 7: Comparison of the nodal errors between linear and modified basis functions

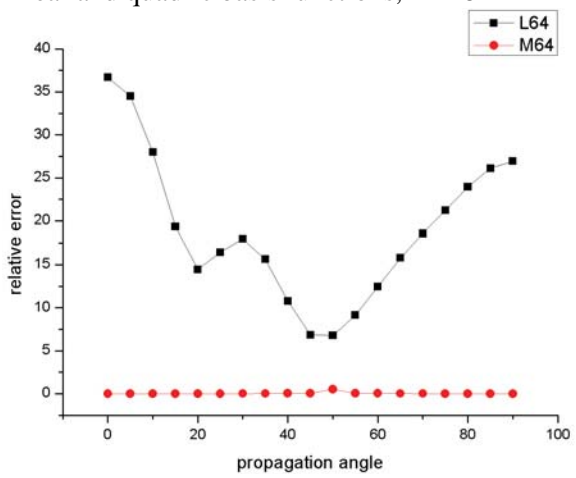

Figure 8: Relative error with respect to propagation angle

single step 0.5, hence, $dinf = 1.5h - 3.0$ for linear basis cases while $dinf = 2.5h - 3.0$ for the modified basis cases. The relative error is defined by Eq. (37). Numerical results are shown in Figs. 3 and 4 for linear and modified basis functions, respectively.

It can be seen from Figs. 3 and 4 that, the size of influence domain has great effect on the numerical results, especially for normal linear basis case. For a given node distribution, there is an optimal radius of influence domain. Smaller radii may lead to inaccuracies and singular coefficient matrix in MLSA, while bigger size of the influence domain will lead to more computational cost. Furthermore, the desired numerical results also lie on the optimal parameters in the implementation of the LBIEM.

5.1.2 Study on the order of monomial basis functions

For low wave number case ($\kappa = 1$) in the above test, linear approximation with 81 nodes gives acceptable accuracy, see fig. 3. In fact, higher order basis functions in MLSA, quadratic basis functions, can give better numerical results, shown in the following Fig.5. But for high wave number cases, say $\kappa = 8$, neither linear (L81) nor quadratic (Q81) basis functions with the 81 nodes can give desired accuracy, see Fig. 6. Here the propagation angle is set $\beta = 45^o$ and the sizes of the influence domain are $dinf = 1.8$.

There is a rule in the simulation of acoustic problems that at least six linear elements or three quadratic elements per wave length are required to obtain enough approximate accuracy, as is done in the acoustic software SYSNOISE. Obviously, for high wave number cases, normal monomial elements (linear, quadratic, or even higher order elements) are largely required, which lead to high computational cost. As a result, modified basis functions possess the special advantage, and only much fewer nodes can attain high accuracy, which can be observed from the following Fig. 7.

5.1.3 Study on the modified basis functions

It can be seen through the comparison between Figs. 3 and 4 that high accuracies can be obtained by adoption of modified basis function. In particular, we choose the results of $49(7 \times 7)$ and $81(9 \times 9)$ node discretizations in section 5.1.1 when the size of the influence domain is $dinf = 1.8$. The node relative errors over the nodes are given in Fig. 7. Obviously, LBIEM solutions with modified basis functions lead to much higher accuracies.

5.1.4 Study on plane wave propagating angles

This section will present numerical results for the relationship between the relative error and the plane wave propagating angle. Here, we adopt the regularly distributed nodes of $64(8 \times 8)$, and choose an optimal radius of influence domain $dinf = 1.8$, based on numerical result in the section 5.1.1. The plane wave propagating angle changes from 0^o to 90^o, i.e., $\beta = 0^o - 90^o$, increasing with single step 5^o. It can be seen from Fig. 8 that when using modified basis functions relative errors keep very low level and are insensitive to the change of wave propagating angle. However, when using linear basis functions the relative errors are sensitive to angle variation and in big level, and the minimal relative error takes place when the propagation angle is close to 45 degrees, which accords well with other literatures' investigation.

5.1.5 Study on wave numbers

In classic FEM, numerical errors increase with approximation and dispersion errors in the high wave number cases. In LBIEM, numerical accuracies are remarkably improved by MLSA with the basis functions modified by plane harmonic wave propagating solutions. A regular nodal distribution of $64(8 \times 8)$ is used to illustrate the numerical accuracies. We choose the size of the influence domain $dinf = 1.8$. Based on the conclusion in reference [see reference [Ihlenburg, F. et al (1995b)], a cut-off value exists for the product κh, where k is the wave number and h is the distance between two close nodes. In this example, the wave number is chosen from 1 to 12, i.e., $\kappa = 1.0 - 12.0$. Numerical results are shown in Fig. 9, where L64 and M64 denote the relative errors with adopted linear and modified basis func-

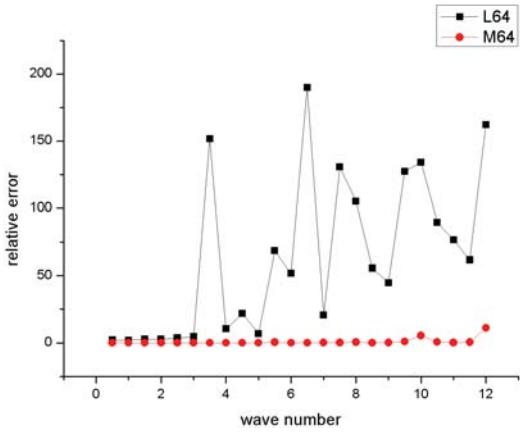

Figure 9: Relative error with respect to wave number

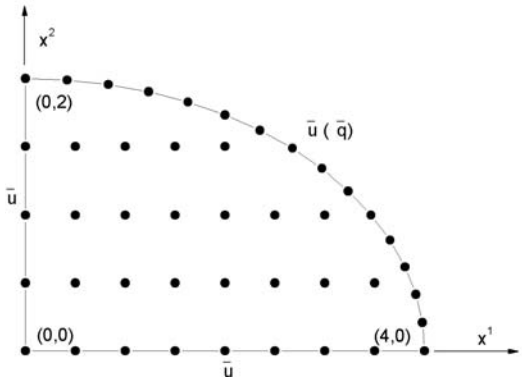

Figure 10: Test example with elliptical boundary

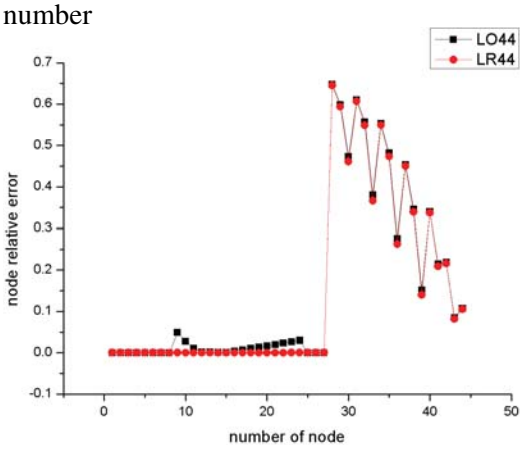

Figure 11: Numerical comparison for linear basis functions and Dirichlet condition on elliptic boundary

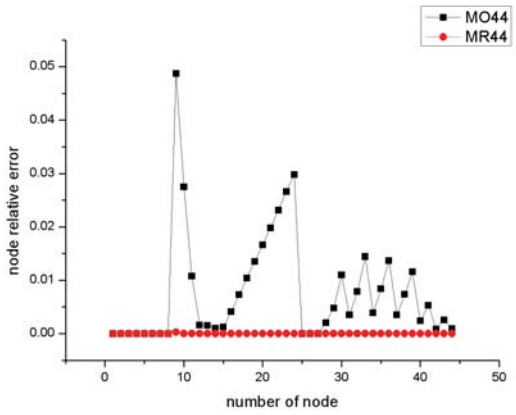

Figure 12: Numerical comparison for modified basis functions and Dirichlet condition on elliptic boundary

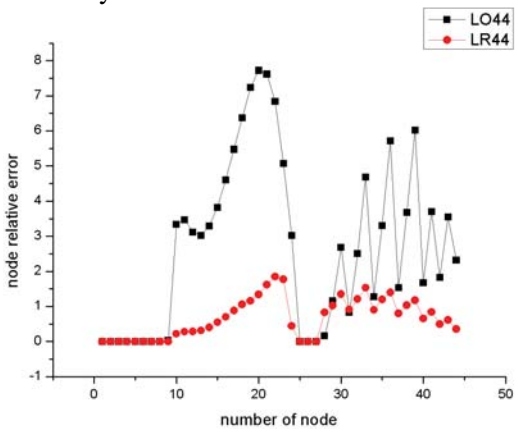

Figure 13: Numerical comparison for linear basis functions and Neumann condition on elliptic boundary

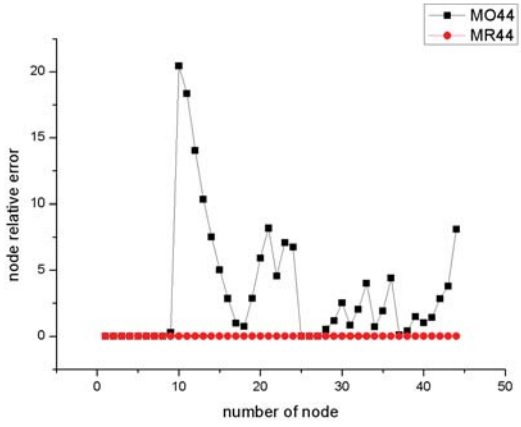

Figure 14: Numerical comparison for modified basis functions and Neumann condition on elliptic boundary

tions, respectively. It can be seen from Fig. 9 that, when using the modified basis functions, numerical results are not sensitive to the wave number and they are in good accuracies, while when using the normal linear basis functions, the relative errors are oscillatory in big range, which also accords with other reference results.

5.2 Comparison between the original LBIEM and the regularized one

For the integration along the local boundary that is also a part of the global boundary, strong singularity will occur except for regular boundary geometries, e.g., straight lines. To show numerical inaccuracies of strongly singular integration, we choose a test example with quarter ellipse domain, see Fig. 10. 44 nodes are distributed in the domain, uniformly. We choose radius of sub-domain $r_0 = 0.005$, size of the influence domain $dinf = 2.0$, plane wave propagating angle $\beta = 45^o$ and wave number $\kappa = 0.5$. Potentials are prescribed on the part of straight boundary, while the potentials or fluxes are prescribed on the elliptical boundary separately. Obviously, singularity will arise when integrating along local boundary coinciding with the elliptical boundary. In Figs. 11-14, L and M denote the results using the linear and modified basis functions, respectively, while O and R represent those using the original and the regularized LBIEs. Numerical comparisons in Figs. 11-14 together with Figs. 4-9 show that regularized LBIEM can present higher computational accuracies, in particular, regularized LBIEM with modified basis functions can present high accuracies and excellent convergence.

5.3 A numerical test with complex boundary

A classic example is introduced in this test, i.e., a car section in two dimensions (see Fig. 15), which boundary is so complex that we can use it to test the program we developed. Note that local boundary L_S inside the domain can be parameterized exactly, but Γ_S is not the case. Here we adopt the polynomial interpolation of 2-th order to approximateΓ_S. Regularized LBIEM and modified basis functions are adopted here. The size of the influence domain is $dinf = 0.5$ and the plane wave propagation angle is 45 degrees. M1 and M2 denote the results when the front panel boundary is Dirichlet or Neumann type, respectively. High accuracies are obtained even though the wave number is high.

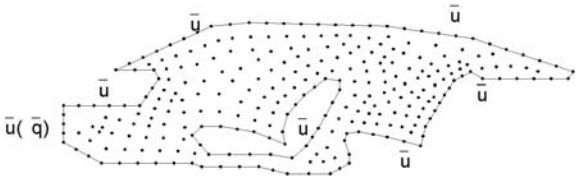

Figure 15: Test example for a car section in two dimensions

However, for the foregoing adoption of modified basis functions, there is a limitation for the practical implementation. The wave number and the propagation angle should be known in advance. For the acoustic field induced by the vibrating structure, we can use the results of vibration analysis for the structure as the acoustic boundary conditions, that is to say, the wave numbers of acoustic wave propagation can be obtained spontaneously while the propagation angles are usually indefinite. We fix the wave propagation angle to 45^o in the modified basis functions, and in the exact solution of the considered problem, the wave propagation angles vary from 0^o to 90^o. The wave number is 3.0 here. From Fig. 17, we can observe that, highly numerical accuracy can be obtained when the wave propagation angle in the exact solution accords with the one in the modified basis functions, and the numerical accuracies may reduce obviously for other cases. Even though we find that the error levels are still acceptable for the general cases.

6 Conclusions

The current paper performs a numerical assessment of the original LBIEM and the regularized LBIEM in acoustic propagation problem governed by Helmholtz equation, especially for high wave number cases. Many parameters, such as the size of the influence domain, the shape controlling parameters, even weight function itself, and so on, should be optimally chosen to get the desired

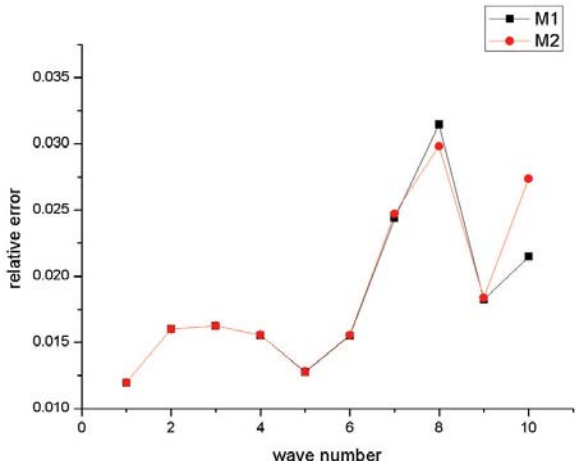

Figure 16: Relative error with respect to wave number for the car section problem

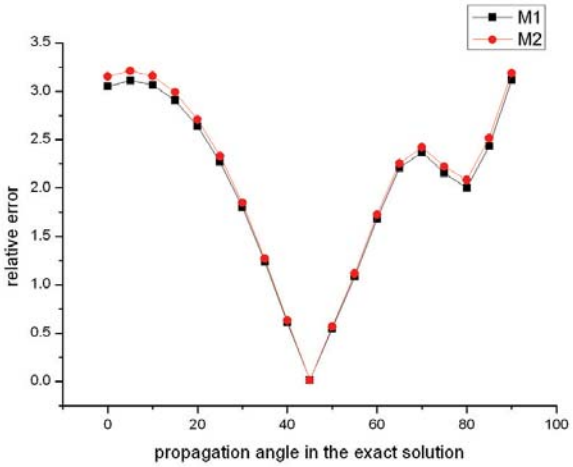

Figure 17: Relative error with respect to propagation angle for the car section problem

computational accuracies. Regularized LBIEM can efficiently deal with the singular integration when the source node locates on the global boundary. Numerical tests show that such improvement is significant. With the implementation of MLSA in the LBIEM, it is natural and convenient to use some special basis functions, which are not easily coped with in the classic FEM. When using basis functions modified with wave propagation solutions, we can obtain the highly numerical accuracies and good convergences in spite of higher wave number cases. In summary, the main contribution of the present paper is the combination of the proposed regularized LBIE formulation with the frequency-dependent basis function in the MLS procedure, and its successful application in the analysis of acoustic wave propagation problems.

It is worth noting that, based on the knowledge of data fitting, MLSA with the basis functions modified with wave propagation solutions can give better local approximation for acoustic propagation problem, in contrast to either the normal monomial basis functions or the interpolation functions in the classical FEM. Therefore, approximation error is greatly decreased even though the same or less nodes are used. Moreover, references [Suleau, S. et al (2000b), Suleau, S. et al (2000a)] drew a conclusion that dispersion error can be also reduced due to implementation of MLSA with modified basis functions. In a word, the obtained high accuracies lie on decrease of both approximation and dispersion errors, especially for high wave number problems. However, there still lack theoretical discussions in interpreting the high numerical accuracies in our implementation of LBIEM, consequently, further investigation is necessary.

Furthermore, it should be pointed out that the present numerical tests are relatively simple and more general cases should be considered in our further investigations. In general, the vibration characters of structures which induce the acoustic propagation may be obtained through simplified numerical analysis and the acoustic characters may be obtained accordingly. By using the acoustic characters in the MLSA approximation, the relevant acoustic wave propagation problem can be solved through appropriate superposition algorithm.

References

Atluri, S. N.; Zhu, T. (1998): A new meshless local Petrov-Galerkin (MLPG) approach in computational mechanics. *Comput. Mech.*, vol. 22, pp. 117-127.

Babuska, I.; Melenk, J. M. (1997): The partition of unity method, *Int. J. Numer. Methods Eng.*, vol. 40, pp. 727-758.

Bouillard, Ph.; Suleau, S. (1998): Element-Free Galerkin solutions for Helmholtz problems: Formulation and numerical assessment of the pollution effect. *Comput. Meth. Appl. Mech. Eng.*, vol. 162, pp. 317-335.

Chen, H. B.; Lu, P.; Huang, M. G.; Williams, F. W. (1998): An effective method for finding values on and near boundaries in the elastic BEM. *Comput. Struct.*, vol. 69, pp. 421-431.

Chen, H. B.; Lu, P.; Schnack, E. (2001): Regularized algorithms for the calculation on and near boundary in 2D elastic BEM. *Eng. Anal. Bound. Elem.*, vol. 25, pp. 851-876.

Chen, H. B.; Yu. D. H.; Schnack, E. (2003): A simple a-posteriori error estimation for adaptive mesh refinement in elastic BEM, *Comput. Mech.*, vol. 30, pp. 343-354.

Ciskowski, R. D.; Brebbia, C. A. (1991): *Boundary Element Methods in Acoustics.* Computational Mechanics Publications, Southampton.

Chen, W. (2002): Meshfree boundary particle method applied to Helmholtz problems. *Eng. Anal. Bound. Elem.*, vol. 26, pp. 577-581.

Chen, W; Hon, Y. C. (2003): Numerical investigation on convergence of boundary knot method in the analysis of homogeneous Helmholtz, modified Helmholtz, and convection–diffusion problems. *Comput. Meth. Appl. Mech. Eng.*, vol 192, pp. 1859-1875.

Deraemaeker, A.; Babuska, I.; Bouillard, P. (1999): Dispersion and pollution of the FEM solution for the Helmholtz equation in one, two and three dimensions. Int. *J. Numer. Methods Eng.*, vol. 46, pp. 471-499.

Guo, X. F.; Chen, H. B.; Wang, N. Y.; Zhang, P. Q. (2006a): Meshless regularized local boundary integral equation method to 2D potential problems. *The Journal of University of Science and Technology of China*; 36(6): 635-640 (in Chinese).

Guo, X. F.; Chen, H. B. (2006b): Dual error indicators for the local boundary integral equation method in 2D potential problems, *Eng. Anal. Bound. Elem.*, vol. 30, pp. 702-708.

Han, Z. D.; Atluri, S. N. (2003): Truly Meshless Local Petrov-Galerkin (MLPG) solutions of traction & displacement BIEs. *CMES: Computer Modeling in Engineering & Sciences*, vol. 4, pp. 665-678.

Han, Z. D.; Rajendran, A. M.; Atluri, S. N. (2005): Meshless Local Petrov-Galerkin (MLPG) approaches for solving nonlinear problems with large deformations and rotations. *CMES: Computer Modeling in Engineering & Sciences*, vol. 10, pp. 1-12.

Ihlenburg, F.; Babuska, I. (1995a): Finite element solution of the Helmholtz equation with high wave number part I: the h-version of the FEM. *Comput. Math. Appl.*, vol. 30, pp. 9-37.

Ihlenburg, F.; Babuska, I. (1995b): Dispersion analysis and error estimation of Galerkin finite element methods for the Helmholtz equation. *Int. J. Numer. Methods Eng.*, vol. 38, pp. 3745-3774.

Sellountos, E. J.; Vavourakis, V.; Polyzos, D. (2005): A new Singular/Hypersingular MLPG(LBIE) method for 2D elastostatics. *CMES: Computer Modeling in Engineering & Sciences*, vol. 7, pp. 35-47.

Sladek, J.; Sladek, V.; Atluri, S. N. (2002a): Application of the local boundary integral equation method to boundary-value problems. *Int. Appl. Mech.*, vol. 38, pp. 1025-1047.

Sladek, J.; Sladek, V.; Keer, R. V. (2002b): Global and local Trefftz boundary integral formulations for sound vibration. *Adv. Eng. Softw.*, vol. 33, pp. 469-476.

Sladek, J.; Sladek, V.; Zhang, C. Z. (2005): A meshless local boundary integral equation method for dynamic anti-plane shear crack problem in functionally graded materials. *Eng. Anal. Bound. Elem.*, vol. 29, pp. 334-342.

Sladek, V.; Sladek, J.; Tanaka, M. (2005): Local integral equations and two meshless polynomial interpolations with application to potential problems in nonhomogeneous media, *CMES: Computer Modeling in Engineering & Sciences*, vol. 7, pp. 69-83.

Sladek, V.; Sladek, J.; Atluri, S. N.; Van Keer, R. (2000): Numerical integration of singularities in meshless implementation of local boundary integral equations. *Comput. Mech.*, vol. 25, pp.

394-403.

Suleau, S.; Deraemaeker, A.; Bouillard, Ph. (2000a): Dispersion and pollution of meshless solutions for the Helmholtz equation. *Comput. Meth. Appl. Mech. Eng.*, vol. 190, pp. 639-657.

Suleau, S.; Bouillard, Ph. (2000b): One-dimensional dispersion analysis for the element-free Galerkin method for the Helmholtz equation. *Int. J. Numer. Methods Eng.*, vol. 47, pp. 1169-1188.

Uras, R. A.; Chang, C. T.; Chen, Y.; Liu, W. K. (1997): Multiresolution reproducing kernel particle methods in acoustics. *J. Comput. Acoust.*, vol. 5, pp. 71-94.

Zhu, T.; Zhang, J. D.; Atluri, S. N. (1998): A local boundary integral equation (LBIE) method in computational mechanics, and a meshless discretization approach. *Comput. Mech.*, vol. 21, pp. 223-235.

Zhu, T.; Zhang, J. D.; Atluri, S. N. (1999): A meshless numerical method based on the local boundary integral equation (LBIE) to solve linear and non-linear boundary value problems. *Eng. Anal. Bound. Elem.*, vol. 23, pp. 375-389.